RSC Advances

PAPER

View Article Online
View Journal | View Issue

Cite this: *RSC Adv.*, 2017, **7**, 10517

RGO/TiO_2 nanosheets immobilized on magnetically actuated artificial cilia film: a new mode for efficient photocatalytic reaction†

Wei Wang,*[ab] Xiaogu Huang,[ab] Min Lai[a] and Chunhua Lu*[bc]

Exploring a proper mode for practical reaction and efficient recycle has been an extensively studied subject in the photocatalysis field. Powder suspension reaction systems and two-dimensional (2D) film reaction systems are insufficient to attain this goal. Herein, we report a systematic study on immobilizing anatase TiO_2 nanosheets on the magnetically actuated artificial cilia film by employing reduced graphene oxide (RGO) as the contact medium. The three-dimensional (3D) artificial cilia film is efficient in immobilizing more powder photocatalysts. When the artificial cilia film is actuated by the rotating magnetic field, the rhodamine B (RhB) degradation efficiency can be greatly improved because of the enhanced mass transfer and product desorption efficiencies. Compared to the static state, a three-fold improvement of the photocatalytic activity is obtained when the magnetic field actuation speed is 800 rpm. Furthermore, 83.1% of the photocatalytic activity is retained after 15 circular reactions, indicating its relative stability. Moreover, RGO conductivity and Au surface plasma resonance (SPR) can further improve the RhB degradation efficiency of 9.0% and 8.8%, respectively. Our findings suggest that this new photocatalysis mode is helpful to apply to, and recycle, the high-reactivity powder photocatalysts.

Received 4th November 2016
Accepted 27th January 2017

DOI: 10.1039/c6ra26306b

rsc.li/rsc-advances

1. Introduction

Photocatalysis is considered as an efficient and green technology in solving environmental contamination and energy supply problems.[1,2] However, the lack of proper application mode blocks its wide practical application. Powder suspension reaction systems and 2D film reaction systems are the most employed application modes in industry.[3–6] Powder suspension reaction systems are efficient in dispersing the photocatalyst particles and improving the contact area, and thus the photocatalysts can sufficiently exert their activities. Recycle and reuse of the photocatalysts are very difficult for nano-sized photocatalysts. Thus, researchers always employ the micro-sized photocatalyst, which has a high aspect ratio and a membrane as the filter to attain the recycle goal. The micro-sized photocatalysts are less reactive than the nano-sized photocatalysts. Thus, this photocatalytic mode is always adopted in the laboratory for activity comparison. On the other hand, 2D photocatalytic film, which is positive for photocatalyst recycle, has been widely investigated in the last few decades. However, mass transfer, light absorption, and specific surface area are greatly limited. Various photocatalytic reactors (*e.g.* light condensing, diffuse reflection and optical fiber types, *etc.*) have been developed to overcome the shortages, but the photocatalytic efficiency is still unsatisfactory. As a result, a new photocatalytic mode employing highly reactive photocatalysts should be discovered.

Among the already discovered semiconductor photocatalysts, anatase TiO_2 is one of the most promising photocatalysts for wide practical application because of its low-cost, environmental friendliness and stability. In the last several years, anatase TiO_2 exposed with highly energetic facets has gained great attention. Particularly, anatase TiO_2 with the {001} and {101} exposed facets is considered to be beneficial in improving the separation efficiency of photo-generated electrons and holes.[7–9] The photocatalytic activity can be improved compared to the traditional TiO_2 exposed with more than 90% of the {101} facet. In order to pursue a much higher photocatalytic activity, noble metals (*e.g.* Au, Pt), graphene, semiconductors, and quantum dots are employed to modify such types of TiO_2.[10–14] Although various and high reactivity photocatalysts have been prepared, the progress of their application is very slow. Thus, researchers have been paying great attention to develop TiO_2 films with exposed {001} facets. To date, two ways have been adopted to attain this goal: (1) *in situ* growth and (2) post heat treatment. Specifically, *in situ* growth is helpful to prepare regular and ordered TiO_2 films with a high percentage

[a]*School of Physics and Optoelectronic Engineering, Nanjing University of Information Science & Technology, Nanjing 210044, PR China. E-mail: wwang@nuist.edu.cn*

[b]*Jiangsu Collaborative Innovation Center for Advanced Inorganic Function Composites, Nanjing Tech University, Nanjing 210009, PR China*

[c]*State Key Laboratory of Materials-Oriented Chemical Engineering, College of Materials Science and Engineering, Nanjing Tech University, Nanjing 210009, PR China*

† Electronic supplementary information (ESI) available. See DOI: 10.1039/c6ra26306b

of exposed {001} facets. Ichimura *et al.* employed the hydrothermal method to grow TiO_2 film exhibiting ~100% {001} reactive facets on the gold substrate.[15] Liao *et al.* anodized TiO_2 nanotube arrays to prepare TiO_2 films consisting of single-crystal nanoparticles with exposed {001} facets.[16] Xiang *et al.* prepared TiO_2 films composed of flower-like TiO_2 microspheres with exposed {001} facets by etching the Ti foil.[17] Sayed *et al.* synthesized the {001} facets TiO_2/Ti film for efficient bezafibrate degradation.[18] All these films are reported to be very reactive, but the film size, yield, light absorption, specific surface area, and costs are unsatisfactory. The post heat treatment method is always based on the already prepared TiO_2 nanosheets. This procedure can easily control the thickness, components, and pore structure of the film.[19] However, the {001} facet, which is always stabilized by F atoms, is thermodynamically unstable. Heat treatments in the air or in aqueous solution do not maintain the {001} facet.[20–22] Moreover, this preparation technology always needs another bond component, reducing the specific surface area of TiO_2 nanosheets. These factors determine that heat treating the TiO_2 nanosheets to extend their practical application seems infeasible.

Based on the above statements, it is urgent to introduce a 3D structure into the photocatalytic film, which can firmly immobilize the TiO_2 nanosheets. Inspired by nature, cilia are efficient in using 3D space and actuating micro-fluid flow.[23–26] For instance, the paramecium has a body-length of *ca.* 100 μm. The cilia, which are 2–15 μm in length, help the paramecium to move forward with a speed of *ca.* 1 mm s^{-1} as a result of high-efficiency micro-fluid mixing. Indeed, there has been an increasing interest in developing such artificial structures to reach various goals.[27,28] Unfortunately, most of the studied cilia structures have a small size.[29] What about developing a self-driven and large-sized artificial cilia film as the photocatalytic matrix?

Herein, we develop a facile method to immobilize the TiO_2 nanosheets onto a magnetic actuated artificial cilia film by employing RGO as the contact medium. Similar to the powder suspension reaction system, the 3D space above the 2D matrix is sufficiently used. Mass transfer and photocatalyst load content can also be improved by the artificial cilia. This strategy also promotes photocatalyst recycle. RhB degradation experiments indicate that there is a positive correlation between the photocatalytic efficiency and the magnetic actuation speed. Depending on the intrinsic property of the cilia film, an optimized magnetic actuating speed of 800 rpm will give the highest photocatalytic activity (a 3-fold improvement). Finally, we prove that RGO and Au SPR are also positive for further improving photocatalytic activity of the cilia film. Our study may establish a bridge between the powder suspension reaction system and the 2D film reaction system, which may promote the practical application of highly reactive powder photocatalysts.

2. Experimental

2.1 Materials

All the adopted reagents, such as dimethylbenzene, ethanol, tetrabutyl titanate, hydrofluoric acid, and (3-aminopropyl) trimethoxysilane (APTMS), were of analytical grade. Distilled water was supplied by Nanjing WanQing Chemical Co., Ltd. Dimethyl siloxane (DMS, Sylgard 184) and its curing agent were supplied by Dow Corning (MI, USA). Cobalt (Co) powder with a particle size of *ca.* 150 nm was purchased from Miyou Company (Nanjing, China). Graphene oxide (GO) aqueous suspension was purchased from Nanjing XFNANO Materials Tech. Co., Ltd.

2.2 Preparation of artificial cilia film

0.15 g Co powder was dispersed in 3 g DMS and 7 g dimethylbenzene, followed by magnetic stirring (300 rpm) for 1 h at room temperature. The curing agent with a 1 : 10 weight ratio to the DMS was added, followed by pouring the suspension into a polytetrafluoroethylene (PTFE) cell with a size of 20 × 20 × 3 mm. The artificial cilia film was obtained after keeping the PTFE cell in a 900 mT perpendicular magnetic field at 60 °C for 24 h.[30,31]

2.3 Immobilization of RGO and TiO_2 nanosheets

Anatase TiO_2 nanosheets with exposed {001} facets were prepared by the hydrothermal method with tetrabutyl titanate and hydrofluoric acid as the reagents.[20] The obtained TiO_2 nanosheets' surfaces were fully adsorbed with F atoms, which were then eliminated completely by washing with aqueous NaOH solution.[32] Finally, the TiO_2 surface is rich in hydrophilic OH groups. Afterwards, 0.2 g TiO_2 was dispersed in 300 mL deionized water, followed by the addition of 2 mL aqueous $HAuCl_4$ solution (1 mmol L^{-1}). The suspension was irradiated with a 300 W xenon lamp for 3 h at room temperature. Purple TiO_2–Au with Au nanoparticles selectively deposited on the {101} facets was obtained.[33] The weight ratio of Au nanoparticles to TiO_2 nanosheets was *ca.* 1%. 0.02 g TiO_2 or TiO_2–Au was then dispersed in 100 mL ethanol, followed by the addition of 1 mL APTMS. After sonication and stirring for 8 h at room temperature, the suspension was centrifuged and re-dispersed in 200 mL ethanol.

The cilia film was pretreated by the air atmospheric pressure glow discharge (AAPGD) to change its surface chemical environment from hydrophobic to hydrophilic.[34] Then, the cilia film was immersed into 3 mL GO aqueous suspension (0.2 mg mL^{-1}). After that, the cilia film was actuated by the magnetic stirrer for 5 min to immobilize GO onto its surface. The GO-wrapped cilia film was immersed into 3 mL of the TiO_2 nanosheets suspension with magnetic actuation for another 5 min, guaranteeing the tight adhesion between the positively charged TiO_2 nanosheets and negatively charged GO. Finally, GO was reduced by the 0.1 M aqueous $NaBH_4$ solution at 80 °C for 1 h to obtain the artificial cilia film immobilized with RGO/TiO_2 nanosheets.[35] For comparison, RGO/TiO_2–Au and pure TiO_2 nanosheets were also immobilized on the artificial cilia film.

2.4 Characterization

X-ray diffraction (XRD) analysis was conducted on an ARL X'TRA X-ray diffractometer using Cu-K_α radiation. Transmission electron microscopy (TEM) and scanning electron microscopy

(SEM) analyses were conducted on the JEOL JEM-2010 electron microscope and Hitachi S-4800 electron microscope, respectively. UV-Vis light absorption spectra were converted from the diffuse reflection spectra and analyzed on the Shimadzu 3101 spectrophotometer with barium sulfate as the reference. Raman spectra were measured on the Labram HR800 spectrometer with the 514 nm laser as the excitation source. Fourier transform infrared (FTIR) spectra were recorded on the Vector-22 spectrometer in the range of 400–4000 cm^{-1}. The wetting property was analyzed on a JGW-360A contact angle meter (Chenghui Testing Machine Co., Ltd., China).

2.5 Photocatalytic experiments

RhB photocatalytic degradation experiments were carried out in a quartz reactor with circulating cooling water and a 500 W xenon lamp as the light source. Typically, 20 mg photocatalyst powder was dispersed in 100 mL RhB (20 mg L^{-1}) aqueous solution for 1 h to reach the adsorption equilibrium. 3 mL RhB aqueous solution was taken out every 30 min to measure the absorption spectrum during the photocatalytic process. The solution was then poured back to continue the photocatalytic reaction. Similarly, the cilia film was immersed in 5 mL RhB aqueous solution, and 1 mL RhB aqueous solution was taken out every 30 min to measure the RhB absorption spectrum. Photo-generated $^{\cdot}OH$ radical was analyzed with a similar procedure based on our previous study.[20] The magnetic field actuation speed (rpm) can be recorded with a commercial frequency meter.

3. Results and discussion

The anatase phase (JCPDS 21-1272) of the as-prepared TiO_2 is evidenced by the XRD analysis (Fig. S1†). SEM and TEM images reveal a sheet-like morphology.[36] All the nanoparticles have a particle size of *ca.* 200 nm and are inclined to aggregate with each other along the [001] direction, resulting in reduced outer surface to contact with the pollutant molecules. The disorder accumulation can also be demonstrated by the XRD analysis because of the (101) diffraction peak being more intense than the (004) diffraction peak.[15,37] Au nanoparticles are photo-deposited on the TiO_2 surface in order to enhance the visible light absorption ability. The TiO_2–Au shows a light absorption peak centered at 560 nm in the range of 400 nm to 800 nm (Fig. 1b). Moreover, the {001}–{101} surface heterojunction also helps the Au nanoparticles to deposit onto the {101} facet (Fig. 1b, inset).[38] Thus, the hot electrons from Au SPR can be used efficiently for photocatalytic reaction.

In order to improve the monodispersity of TiO_2 nanosheets, we employ the artificial cilia film as the supporter. Fig. 2a and b show the top view and the front view, respectively, of the cilia film. The black color and rough surface of the cilia film originate from the Co particles, which are wrapped by the PDMS. It can be observed that there are vertical cilia located on the 2D flat matrix. Typical SEM image indicates that the distance between every cilium is *ca.* 300 μm (Fig. 3a). Because of the elastic property of PDMS, the cilia film can accommodate a large deformation when a weak force is applied (Fig. 3b). Moreover, the vertical cilia will rotate in a circular path when actuated by a magnetic stirrer (Fig. 2c and d). The weak perturbation is helpful to perturb the fluid and improve mass transfer during the photocatalytic process.

In order to immobilize the hydrophilic TiO_2 nanosheets and GO onto the artificial cilia film, the hydrophobic surface of PDMS should be changed. The static contact angle of the water droplet on the PDMS film is changed from 88° to less than 5° with the help of AAPGD treatment (Fig. S2a and b†). Thus, the

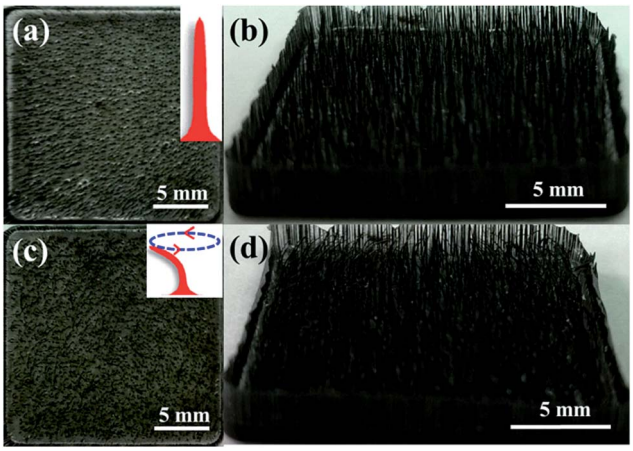

Fig. 2 (a and c) Top view and (b and d) front view of the artificial cilia film at the static state (a and b) and dynamic state (c and d).

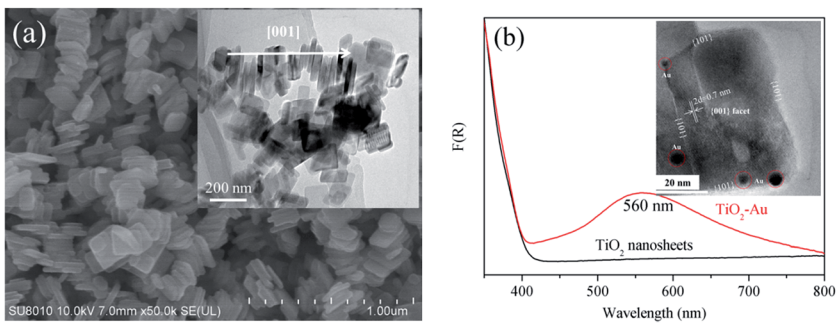

Fig. 1 (a) Morphology of the as-prepared TiO_2 nanosheets. (b) Light absorption spectra of TiO_2 nanosheets and TiO_2–Au. TEM image of TiO_2–Au indicates that the Au nanoparticles are deposited on the {101} facet ((b), inset).

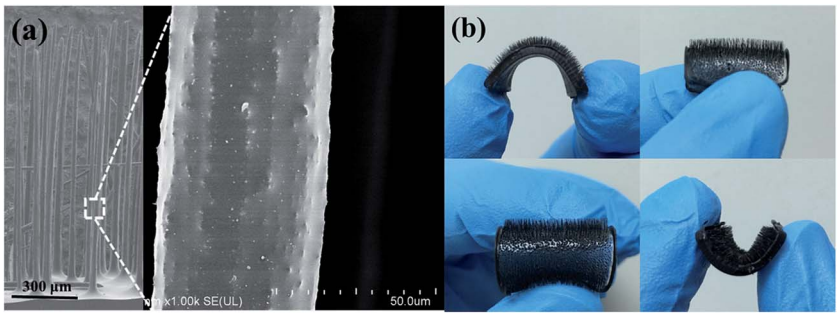

Fig. 3 (a) SEM image and (b) photographs of deformation of the artificial cilia film.

hydrophilic GO can be wrapped firmly on the cilia surface (Fig. 4a). Because of the soft property and 2D structure of GO, numerous wrinkles are formed on the cilia outer surface.

As shown in Scheme 1, we employed APTMS to modify the TiO_2 nanosheets. The APTMS molecules can react with the TiO_2 nanosheets because the surface-adsorbed F atoms have been replaced by OH groups. Then, the APTMS-modified TiO_2 nanosheets can be homogeneously and stably suspended in ethanol for more than 30 days because of the repulsive interaction among the $-NH_2$ groups (Fig. S3,† inset). We found that this surface modification has little negative effect on the photocatalytic activity (Fig. S3†). The slight decrease may due to the blocking role of the APTMS molecules between the TiO_2 surface and RhB molecules. In order to clarify the specific reaction among TiO_2 nanosheets, APTMS, and RGO, we employed the powder samples for the FTIR analysis (Fig. 4b). When GO aqueous solution is added into the TiO_2 suspension drop by drop, they will quickly contact with each other because of the electrostatic adhesion between the $-NH_2$ groups and GO whose surface is rich in –OH and –COOH groups. After $NaBH_4$ reduction, the O=C–NH– group will be formed to enhance the interaction between RGO and TiO_2 nanosheets. Specifically, the absorption band in the range of 400 cm^{-1} to 600 cm^{-1} is the characteristic Ti–O–Ti vibration of TiO_2 nanosheets. After APTMS modification, this absorption band is broadened and red shifted. The typical O–H absorption band at 3455 cm^{-1} of TiO_2 nanosheets is also shifted to 3417 cm^{-1} because of the introduced N–H vibration. The formed Si–O–Ti chemical bond has an absorption band at 933 cm^{-1}, indicating the tight interaction between APTMS and TiO_2 nanosheets. The

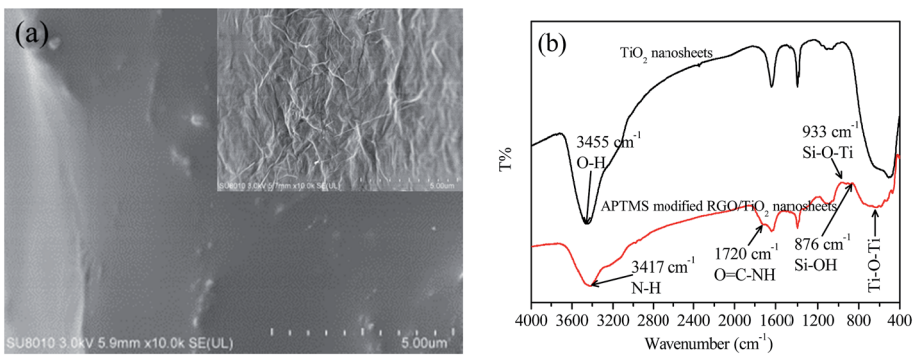

Fig. 4 (a) SEM images of pristine and GO wrapped (inset) cilia. (b) FTIR spectra of TiO_2 nanosheets and APTMS-modified RGO/TiO_2 nanosheets.

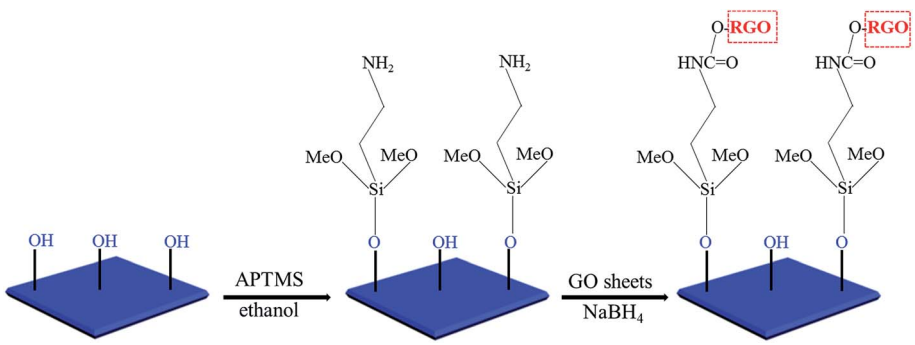

Scheme 1 Schematic of the interaction among APTMS, TiO_2 nanosheets, and RGO.

absorption band of O=C–NH–, which originates from APTMS and GO reaction, is found at 1720 cm^{-1}. We speculated that the amidation is partial because the reaction system is rich in water. Moreover, the final structure, shown in Scheme 1, cannot last for a long time because of the partial hydrolysis of APTMS in ambient environment, which can be demonstrated by the Si–OH vibration band at 876 cm^{-1}. Nevertheless, the strong interaction is positive for RGO and TiO_2 immobilization. Thus most of the cilia surface is covered by the RGO and TiO_2 nanosheets (Fig. 5a). In contrast, little TiO_2 is immobilized on the cilia without RGO as the contact medium, which may also reduce the immobilization stability (Fig. 5b). Most importantly, the pristine structure of TiO_2 nanosheets is well-maintained, which is beneficial for efficient photocatalytic reaction.

RhB is employed as a typical organic dye to evaluate the photocatalytic activity of the artificial cilia film. Interestingly, the magnetic actuation speed plays a vital role in influencing the photocatalytic activities. As shown in Fig. 6a, the cilia film at the static state has an inherent ability for RhB degradation because of the existence of TiO_2 nanosheets. RhB degradation efficiency is evidently improved when magnetic actuation is applied. During this process, the cilia give a slight deformation and rotate along with the magnetic stirrer. Thus, the mass transfer efficiency is greatly improved.[31] Our results indicate that 800 rpm is the optimized actuation speed for the most effective RhB degradation. A three-fold improvement is obtained compared to that at the static state. However, a much higher actuation speed does not further improve the photocatalytic efficiency. The flexible cilia can truly rotate along with the variable magnetic field, but its inherent properties determine that the cilia rotation frequency cannot be increased indefinitely. Thus, an actuation speed higher than 800 rpm will disturb the regular rotation, resulting in reduced mass transfer. This speculated law is also evidenced by the $^{\bullet}OH$ radical generation analysis (Fig. 6b); these are formed by the photogenerated electrons and holes of the excited TiO_2. The highest PL emission intensity indicates that most $^{\bullet}OH$ radicals are generated at the 800 rpm actuation speed. Interestingly, the light absorption spectra of the cilia film are the same at both static state and dynamic state (Fig. S4†), indicating that the activity improvement has little relationship with the light absorption. Next, we try to evaluate the activity durability of the artificial cilia film. The photocatalytic activity of the cilia film is relatively stable. 83.1% of the photocatalytic activity is retained after 15 circular reactions (Fig. S5†). As is well known, TiO_2 is very stable under the light irradiation. The 16.9% activity decrease may be due to the TiO_2 desorption from the cilia. A typical SEM image (Fig. S6a†) indicates that the TiO_2 nanosheets density is lower than that of the pristine situation after 15 cycles (Fig. 5a). Interestingly, some areas without the RGO are blank, and the TiO_2 nanosheets are located on the RGO edges (Fig. S6b†). Recently, we have been trying to solve the adhesion problem and get a much more stable immobilization structure.

We further evaluate the positive effect of RGO and Au nanoparticles at the actuation speed of 800 rpm. Specifically, Fig. S7† shows the Raman spectra of GO and RGO. The integrated intensity ratio of the D band to the G band (I_D/I_G) is decreased from 1.7 for GO to 1.3 for RGO, indicating its less sp^3

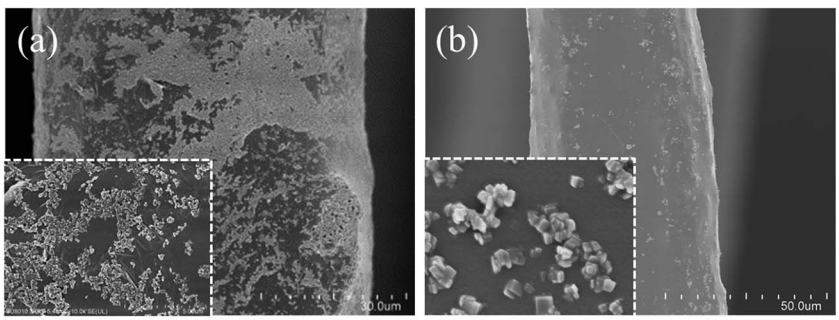

Fig. 5 SEM images of AAPGD-treated cilia immobilized with (a) RGO/TiO_2 nanosheets and (b) pure TiO_2 nanosheets.

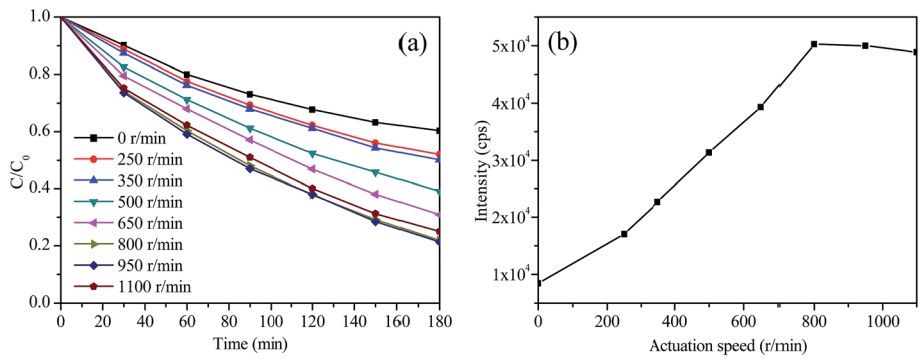

Fig. 6 (a) RhB photocatalytic degradation efficiencies (b) $^{\bullet}OH$ generation analysis of the artificial cilia film at different magnetic actuation speeds.

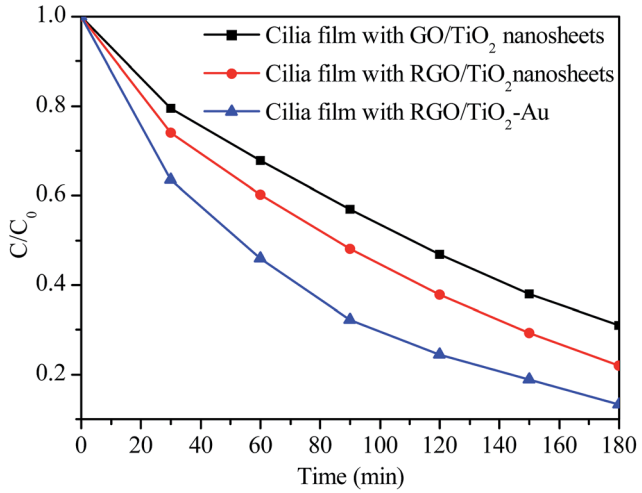

Fig. 7 RhB degradation efficiencies of the artificial cilia film immobilized with GO/TiO_2 nanosheets, RGO/TiO_2 nanosheets, and RGO/TiO_2–Au at a magnetic actuation speed of 800 rpm.

carbon defects and more sp^2 carbon. The reduction process is beneficial in improving the electrical conduction of GO, and thus the RhB degradation efficiency can be improved by *ca.* 9% (Fig. 7). Moreover, when Au nanoparticles are selectively deposited on the {101} facet, the Au SPR effect further improves the visible light utilization efficiency. Another 8.8% improvement is obtained when the artificial cilia film is immobilized with RGO/TiO_2–Au. These results indicate that employing the function materials, such as RGO and Au, is important for further improving the photocatalytic efficiency of the cilia film.

4. Conclusion

We conduct a systematic study on magnetically actuated 3D artificial cilia film toward a new mode for efficient photocatalytic reaction. Anatase TiO_2 nanosheets with exposed {001} facets are employed as the typical high-reactivity photocatalyst to verify our viewpoint. With the help of RGO as the contact medium, TiO_2 nanosheets can be immobilized stably on the artificial cilia film, resulting in a relatively stable photocatalytic activity. We find that the magnetic field actuation speed has a close relationship with the mass transfer and product desorption efficiency. The optimized RhB degradation efficiency is obtained when the magnetic field actuation speed is 800 rpm. Functional materials such as RGO and Au nanoparticles are also important factors in improving the photocatalytic activity. The new and efficient photocatalytic mode may bridge the gap between powder suspension reaction systems and 2D film reaction systems. Our findings provide a new insight into the practical application of highly reactive, nano-sized powder photocatalysts.

Acknowledgements

This study was supported by the National Natural Science Foundation of China (No. 51502143), Natural Science Foundation of Jiangsu Province (No. BK20150919), Key University Science Research Project of Jiangsu Province (No. 15KJB430022), and the Startup Foundation for Introducing Talent of NUIST (2014r037).

References

1 J. Liu, Y. Liu, N. Y. Liu, Y. Z. Han, X. Zhang, H. Huang, Y. Lifshitz, S. T. Lee, J. Zhong and Z. H. Kang, Metal-free efficient photocatalyst for stable visible water splitting *via* a two-electron pathway, *Science*, 2015, **347**, 970–974.
2 M. Zhang, W. Jiang, D. Liu, J. Wang, Y. Liu, Y. Zhu and Y. Zhu, Photodegradation of phenol *via* C_3N_4–agar hybrid hydrogel 3D photocatalysts with free separation, *Appl. Catal., B*, 2016, **183**, 263–268.
3 Y. J. Zhang, L. C. Liu, L. L. Ni and B. L. Wang, A facile and low-cost synthesis of granulated blast furnace slag-based cementitious material coupled with Fe_2O_3 catalyst for treatment of dye wastewater, *Appl. Catal., B*, 2013, **138**, 9–16.
4 B. Y. Lee, A. R. Jayapalan, M. H. Bergin and K. E. Kurtis, Photocatalytic cement exposed to nitrogen oxides: Effect of oxidation and binding, *Cem. Concr. Res.*, 2014, **60**, 30–36.
5 R. Fateh, R. Dillert and D. Bahnemann, Preparation and characterization of transparent hydrophilic photocatalytic TiO_2/SiO_2 thin films on polycarbonate, *Langmuir*, 2013, **29**(11), 3730–3739.
6 R. Fateh, A. A. Ismail, R. Dillert and D. W. Bahnemann, Highly active crystalline mesoporous TiO_2 films coated onto polycarbonate substrates for self-cleaning applications, *J. Phys. Chem. C*, 2011, **115**(21), 10405–10411.
7 T. Tachikawa, T. Ochi and Y. Kobori, Crystal-face-dependent charge dynamics on a $BiVO_4$ photocatalyst revealed by single-particle spectroelectrochemistry, *ACS Catal.*, 2016, 2250–2256.
8 D. Sun, W. Yang, L. Zhou, W. Sun, Q. Li and J. K. Shang, The selective deposition of silver nanoparticles onto {101} facets of TiO_2 nanocrystals with co-exposed {001}/{101} facets, and their enhanced photocatalytic reduction of aqueous nitrate under simulated solar illumination, *Appl. Catal., B*, 2016, **182**, 85–93.
9 J. D. Peng, C. M. Tseng, R. Vittal and K. C. Ho, Mesoporous anatase-TiO_2 spheres consisting of nanosheets of exposed (001)-facets for $[Co(bpy)_3]^{2+/3+}$ based dye-sensitized solar cells, *Nano Energy*, 2016, **22**, 136–148.
10 W. K. Wang, J. J. Chen, W. W. Li, D. N. Pei, X. Zhang and H. Q. Yu, Synthesis of Pt-loaded self-interspersed anatase TiO_2 with a large fraction of (001) facets for efficient photocatalytic nitrobenzene degradation, *ACS Appl. Mater. Interfaces*, 2015, **7**(36), 20349–20359.
11 W. Wang, Y. J. Zhou, Y. R. Ni, C. H. Lu and Z. Z. Xu, Superiority and mechanism of Pt oriented-deposition in improving the photocatalytic activity of TiO_2 sphere with exposed {001} facet, *Mater. Lett.*, 2015, **145**, 180–183.
12 L. Pan, J. J. Zou, S. Wang, Z. F. Huang, A. Yu, L. Wang and X. Zhang, Quantum dot self-decorated TiO_2 nanosheets, *Chem. Commun.*, 2013, **49**(59), 6593–6595.
13 B. Jiang, C. Tian, Q. Pan, Z. Jiang, J. Q. Wang, W. Yan and H. Fu, Enhanced photocatalytic activity and electron

transfer mechanisms of graphene/TiO_2 with exposed {001} facets, *J. Phys. Chem. A*, 2011, **115**(48), 23718–23725.

14 J. J. Chen, W. K. Wang, W. W. Li, D. N. Pei and H. Q. Yu, Roles of crystal surface in Pt-loaded titania for photocatalytic conversion of organic pollutants: A first-principle theoretical calculation, *ACS Appl. Mater. Interfaces*, 2015, **7**(23), 12671–12678.

15 A. S. Ichimura, B. M. Mack, S. M. Usmani and D. G. Mars, Direct synthesis of anatase films with ~100% (001) facets and [001] preferred orientation, *Chem. Mater.*, 2012, **24**(12), 2324–2329.

16 Y. Liao, H. Zhang, W. Que, P. Zhong, F. Bai, Z. Zhong, Q. Wen and W. Chen, Activating the single-crystal TiO_2 nanoparticle film with exposed {001} facets, *ACS Appl. Mater. Interfaces*, 2013, **5**(14), 6463–6466.

17 Q. Xiang, J. Yu and M. Jaroniec, Tunable photocatalytic selectivity of TiO_2 films consisted of flower-like microspheres with exposed {001} facets, *Chem. Commun.*, 2011, **47**(15), 4532–4534.

18 M. Sayed, P. Fu, L. A. Shah, H. M. Khan, J. Nisar, M. Ismail and P. Zhang, VUV-photocatalytic degradation of bezafibrate by hydrothermally synthesized enhanced {001} facets TiO_2/Ti film, *J. Phys. Chem. A*, 2016, **120**(1), 118–127.

19 W. Wang, H. Zhang, R. Wang, M. Feng and Y. Chen, Design of a TiO_2 nanosheet/nanoparticle gradient film photoanode and its improved performance for dye-sensitized solar cells, *Nanoscale*, 2014, **6**(4), 2390–2396.

20 W. Wang, C. H. Lu, Y. R. Ni and Z. Z. Xu, Crystal facet growth behavior and thermal stability of {001} faceted anatase TiO_2: mechanistic role of gaseous HF and visible-light photocatalytic activity, *CrystEngComm*, 2013, **15**(13), 2537–2543.

21 K. Lv, Q. Xiang and J. Yu, Effect of calcination temperature on morphology and photocatalytic activity of anatase TiO_2 nanosheets with exposed {001} facets, *Appl. Catal., B*, 2011, **104**(3–4), 275–281.

22 X. H. Yang, Z. Li, C. Sun, H. G. Yang and C. Li, Hydrothermal stability of {001} faceted anatase TiO_2, *Chem. Mater.*, 2011, **23**(15), 3486–3494.

23 C. Y. Chen, C. Y. Chen, C. Y. Lin and Y. T. Hu, Magnetically actuated artificial cilia for optimum mixing performance in microfluidics, *Lab Chip*, 2013, **13**(14), 2834–2839.

24 A. Keißner and C. Brücker, Directional fluid transport along artificial ciliary surfaces with base-layer actuation of counter-rotating orbital beating patterns, *Soft Matter*, 2012, **8**(19), 5342–5349.

25 S. N. Khaderi, C. B. Craus, J. Hussong, N. Schorr, J. Belardi, J. Westerweel, O. Prucker, J. Ruhe, J. M. den Toonder and P. R. Onck, Magnetically-actuated artificial cilia for microfluidic propulsion, *Lab Chip*, 2011, **11**(12), 2002–2010.

26 F. Fahrni, M. W. J. Prins and L. J. van Ijzendoorn, Micro-fluidic actuation using magnetic artificial cilia, *Lab Chip*, 2009, **9**(23), 3413–3421.

27 C. J. Campbell and B. A. Crzybowski, Microfluidic mixers: from microfabricated to self-assembling devices, *Science*, 2004, **362**, 1069–1086.

28 P. Schroeder, J. Schotter, A. Shoshi, M. Eggeling, O. Bethge, A. Hütten and H. Brückl, Artificial cilia of magnetically tagged polymer nanowires for biomimetic mechanosensing, *Bioinspiration Biomimetics*, 2011, **6**(4), 046007.

29 Y. Wang, Y. Gao, H. Wyss, P. Anderson and J. Den Toonder, Out of the cleanroom, self-assembled magnetic artificial cilia, *Lab Chip*, 2013, **13**(17), 3360–3366.

30 F. P. Peng, Q. Zhou, D. P. Zhang, C. H. Lu, Y. R. Ni, J. H. Kou, J. Wang and Z. Z. Xu, Bio-inspired design: Inner-motile multifunctional ZnO/CdS heterostructures magnetically actuated artificial cilia film for photocatalytic hydrogen evolution, *Appl. Catal., B*, 2015, **165**, 419–427.

31 D. P. Zhang, W. Wang, F. P. Peng, J. H. Kou, Y. R. Ni, C. H. Lu and Z. Z. Xu, A bio-inspired inner-motile photocatalyst film: a magnetically actuated artificial cilia photocatalyst, *Nanoscale*, 2014, **6**(10), 5516–5525.

32 J. G. Yu, L. F. Qi and M. Jaroniec, Hydrogen production by photocatalytic water splitting over Pt/TiO_2 nanosheets with exposed (001) facets, *J. Phys. Chem. C*, 2010, **114**(30), 13118–13125.

33 R. Li, F. Zhang, D. Wang, J. Yang, M. Li, J. Zhu, X. Zhou, H. Han and C. Li, Spatial separation of photogenerated electrons and holes among {010} and {110} crystal facets of $BiVO_4$, *Nat. Commun.*, 2013, **4**, 1432.

34 F. Peng, Y. Ni, Q. Zhou, J. Kou, C. Lu and Z. Xu, Fabrication of a flexible graphene–TiO_2/PDMS photocatalytic film by combining air atmospheric pressure glow discharge treatment, *Chem. Eng. Process.*, 2016, **101**, 8–15.

35 J. T. Han, B. J. Kim, B. G. Kim, J. S. Kim, B. H. Jeong, S. Y. Jeong, H. J. Jeong, J. H. Cho and G. W. Lee, Enhanced electrical properties of reduced graphene oxide multilayer films by *in situ* insertion of a TiO_2 Layer, *ACS Nano*, 2011, **5**(11), 8884–8891.

36 W. Wang, Y. R. Ni, C. H. Lu and Z. Z. Xu, Hydrogenation of TiO_2 nanosheets with exposed {001} facets for enhanced photocatalytic activity, *RSC Adv.*, 2012, **2**(22), 8286–8288.

37 H. Xu, P. Reunchan, S. Ouyang, H. Tong, N. Umezawa, T. Kako and J. Ye, Anatase TiO_2 single crystals exposed with high-reactive {111} facets toward efficient H_2 evolution, *Chem. Mater.*, 2013, **25**(3), 405–411.

38 J. G. Yu, J. X. Low, W. Xiao, P. Zhou and M. Jaroniec, Enhanced photocatalytic CO_2-reduction activity of anatase TiO_2 by coexposed {001} and {101} facets, *J. Am. Chem. Soc.*, 2014, **136**(25), 8839–8842.